Reaction Diffusion Patterns in the Catalytic CO-oxidation on Pt(110): Front Propagation and Spiral Waves

ARTICLE *in* THE JOURNAL OF CHEMICAL PHYSICS · JUNE 1993

Impact Factor: 2.95 · DOI: 10.1063/1.464323

Reaction diffusion patterns in the catalytic CO-oxidation on Pt(110): Front propagation and spiral waves

S. Nettesheim, A. von Oertzen, H. H. Rotermund, and G. Ertl
Fritz-Haber-Institut der Max-Planck-Gesellschaft, Faradayweg 4-6, W-1000 Berlin 33, Germany

(Received 29 December 1992; accepted 5 March 1993)

The dynamic behavior of elliptical front propagation and spiral-shaped excitation concentration waves associated with the catalytic oxidation of CO on a Pt(110)-surface was investigated by means of photoemission electron microscopy (PEEM). The properties of these patterns can be tuned through the control parameters, viz., the partial pressures of CO and O_2 and the sample temperature. Over a wide range of control parameters the transition between two metastable states (CO_{ad} and O_{ad} covered surface) proceeds via nucleation and growth of elliptical reaction-diffusion (RD)-fronts. Front velocities and critical radii for nucleation are determined by the diffusion of adsorbed CO under reaction conditions. If at constant p_{O_2}, T the CO partial pressure is increased beyond a critical value a transition to qualitatively different dynamic behavior takes place. The elliptical fronts give way to oxygen spiral waves of excitation spreading across the CO-covered areas. For fixed experimental conditions a broad distribution of spatial wavelengths and temporal rotation periods was found. This effect has to be attributed to the existence of surface defects of μm-size to which the spiral tip is pinned. These data lead to a dispersion relation between the front propagation velocity and the wavelength, respectively, period. In addition, the dynamics of free spiral-shaped excitation waves was investigated under the influence of externally modulated temperature. Now the spiral starts to drift, resulting in distortion of the Archimedian shape and a pronounced Doppler effect.

I. INTRODUCTION

The isothermal catalytic oxidation of CO on a Pt(110) surface under steady flow conditions was found to exhibit a large variety of spatio-temporal concentration patterns which were visualized with photoemission electron microscopy (PEEM).[1–3] The mechanism of catalytic CO oxidation on surfaces of the platinum group metals has been well established and proceeds through the following steps:[4]

$$CO + * \rightleftarrows CO_{ad},$$

$$O_2 + 2* \rightarrow 2O_{ad},$$

$$CO_{ad} + O_{ad} \rightarrow CO_2 + 2*,$$

where * denotes schematically a free adsorption site which has, however, a different meaning for the two adsorbates. CO has a tendency for the formation of densely packed adlayers which inhibit the dissociative adsorption of oxygen, while the adsorbed O atoms on the other hand form rather open surface configurations which do not noticeably affect the additional adsorption of CO. The associated kinetic equations lead to bistability as explored, e.g., in detail for Pt(111), for which system also phenomena of wave front propagation were treated theoretically by inclusion of surface diffusion of the adsorbed CO molecules.[5]

With the more open Pt(110) surface the situation is more complex. Over a narrow range of parameters the kinetics becomes oscillatory and even chaotic which has to be attributed to the CO driven reversible structural transformation of the Pt(110) surface which is associated with a variation of the oxygen sticking coefficient and hence of the reactivity.[6] The oscillatory temporal behavior could be successfully modeled by solution of a set of ordinary differential equations (ODE's) derived on the basis of the experimental evidence on the individual steps involved.[7] The associated bifurcation diagram reveals, apart from the oscillatory regime, also ranges of parameters for which the system becomes bistable or excitable. Experimentally, various phenomena of spatio-temporal self-organization could be observed; bistability showing the transition of an O-covered to a CO-covered surface (or vice versa) through the growth of elliptical RD-fronts as well as excitability dominated by the spread of target patterns, spiral waves, and solitary pulses. Self-sustained oscillatory behavior is also observed over a wide control parameter range which is usually associated with standing concentration waves. Coupling between different areas is either dominated by reaction-diffusion or globally through the gas phase.[1–3]

This paper will focus on excitability and the growth of spiral waves. The close relationship of spatio-temporal patterns in the catalytic CO oxidation on single crystal surfaces to pattern formation in other chemical or biological systems far from equilibrium demonstrates the universality of the underlying dynamical models. The main advantage of the system presented here are its pure two-dimensional character, the transparency of the elementary steps involved in the reaction dynamics, and the wide range of accessible control parameters.

II. EXPERIMENT

Experiments were carried out in a standard turbomolecular pumped ultrahigh vacuum (UHV)-system operated as a constant flow reactor. During reaction the partial pressures of the reactants (CO and O_2) were accurately adjusted by a feedback-stabilized gas inlet system con-

stantly pumped with $\sim 200\ \ell/s$. Operation in the low pressure regime ($<10^{-3}$ mbar) ensured a gradient-free flow and low reaction rates necessary to satisfy isothermal reaction conditions. Temperature was measured by a Chromel–Alumel thermocouple. The thermocouple was connected to a feedback-controlled power supply constantly heating a tungsten filament on the backside of the sample.

The surface ($8\times 12\ mm^2$) of the Pt(110) single crystal was cleaned by oxidation, Ar ion bombardment, and subsequent annealing to 1000 K. Carbonaceous surface impurities with concentrations below the Auger detection limit were reactively removed by heating up the sample with coadsorbed oxygen monitoring the CO desorption signal with a quadrupole mass spectrometer. This cycle was repeated until CO desorption could no longer be found. The structural perfection of the surface including the reversible CO induced phase transition $1\times 2\rightarrow 1\times 1$ was checked with low energy electron diffraction (LEED).

The photoemission electron microscope (PEEM), as developed by Engel *et al.*,[8] was used to visualize the spatio-temporal concentration patterns with a lateral resolution down to 0.5 μm and a temporal resolution limited to 20 ms using standard video technique. In the images to be shown, oxygen covered areas will be dark due to the high work function of the O_{ad} covered Pt(110) surface ($\Phi=6.5$ eV), CO-covered areas ($\Phi=5.8$ eV) will be characterized by a medium shade of gray, and the clean surface ($\Phi=5.5$ eV) will appear bright.[9]

III. RESULTS AND DISCUSSION

A. General phenomenology

Generally, a bistable system can, for a given set of control parameters, be in two states which are stable against small perturbations while transitions between these states are initiated by stronger perturbations. This transition is mediated through nucleation and growth of reaction/diffusion fronts. With the present system, the surface may be in states which are characterized by predominant coverage with either adsorbed CO or O. However, with the Pt(110) surface no simple bistability is observed experimentally. Nucleation of CO islands on an O coverage area and vice versa occurs in the normal way and leads at first to the growth of patches which are elliptical in shape because of the anisotropy of the surface diffusion coefficients.[10] However, after some time both the CO and O-covered patches lose stability. Growing CO-fronts on O-covered surrounding coexist with O-fronts on the CO-covered parts of the surface and the overall ratio of O to CO coverage varies continuously with time, while with a simple bistable system the transformation would be completely irreversible. With the present system, however, the overall ratio of the two coverages varies with time in an irregular manner. In a simplified picture, this behavior can be traced back to the slow kinetics of the structural transformation of the Pt(110) surface which continuously reduces the stability of a spreading state until a defect can trigger the reverse transition. This special case demonstrates that in the presence of local inhomogeneities a distributed bistable system can exhibit metastable behavior including even overall rate variations which should not be confused with the occurrence of true self-sustained rate oscillations.[11]

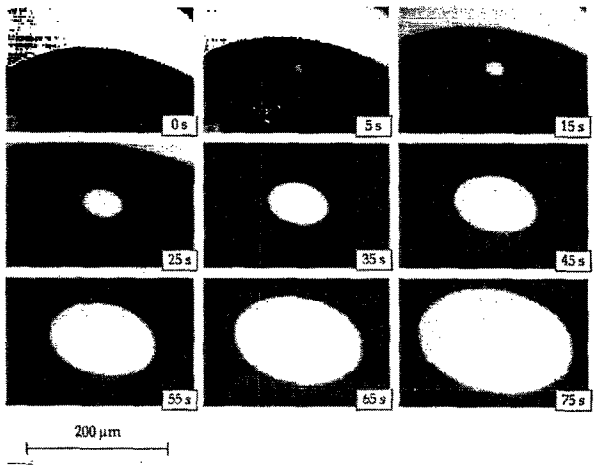

FIG. 1. PEEM images reflecting nucleation and growth of a CO-front (bright areas) on a Pt(110) surface during catalytic CO oxidation at $T=443$ K, $p_{O_2}=4\times 10^{-4}$ mbar, $p_{CO}=3.6\times 10^{-5}$ mbar. The propagation velocity of the CO-front is 1.5 μm/s along the [110]-direction and 0.8 μm/s along the [001]-direction. A coexisting O-front spreads with 2.8 μm/s along [110] and with 1.5 μm/s along [001].

As an example, Fig. 1 shows the nucleation and growth of a CO wave inside an O region while simultaneously an oxygen wave propagates into a CO-covered region. No collective effects in the growth of individual waves was observed so that each of them could be analyzed separately. It should be mentioned, however, that the small variations of the partial pressures associated with overall rate oscillations may provide an efficient global coupling mechanism between different areas on the surface. Hence it has to be concluded that any variations in the overall catalytic activity might also effect the wave propagation velocities which effect was, however, found to be negligible for the data to be presented here.

If under steady-state flow conditions one of the control parameters is varied in a manner that the threshold to excitability is reached, the reversible CO-induced structural transformation of the surface gives rise to a negative feedback which may lead to the propagation of concentration pulses or spirals. If one assumes that a small element within the more reactive 1×1-phase is perturbed so that the (local) CO coverage decreases below a critical value, enhanced oxygen adsorption will lead to reactive removal of CO from adjacent patches. The 1×1-phase will be no longer stable and transforms into the 1×2-structure. Here the oxygen sticking coefficient is lower, adsorbed O atoms will be reacted off and displaced by CO, the 1×1-phase is restored and the cycle can be triggered again.

Spatial coupling is introduced through the diffusional flow of CO between neighboring surface elements, so that a burst of activity can spread over the surface. In contrast to the growth of reaction-diffusion (RD)-fronts in the

bistable regime, with spiral waves traveling waves can pass many times through the same region. The migration of adsorbed oxygen atoms can be neglected compared to the diffusion of CO.[12] In analogy to the predominantly CO-covered surface also the reactive oxygen covered state exhibits excitability accompanied with the spread of CO-pulses of excitation. Experimentally the latter exist only in a narrow range of control parameters. CO-pulses on the oxygen covered surface are found to be less stable than their counterparts on the CO-covered surface. This asymmetry has to be attributed to the fact that an O_{ad} covered surface never inhibits noticeably CO adsorption and hence a CO pulse may spread on an oxygen covered surface close to the threshold of the 1×2–1×1 phase transition. The latter acts as inhibitor for further CO adsorption so that the pulse width is narrow and the excitation is easily damped out.

Spirals are among the most stable autonomous wave patterns in excitable media. Their existence is not necessarily coupled to the presence of local inhomogeneities. For the catalytic CO-oxidation on the Pt(110) surface a large variety of spiral waves has been observed and theoretical analysis has already been performed to some extent both analytically and in computer simulations.[13] The properties of spiral waves can nicely be tuned through the control parameters. At sufficiently high excitability of the medium the spiral tip rotates around a spatially fixed core of finite size.

Although diffusion is responsible for spatial coupling in the range of the diffusion length ($\langle x^2\rangle = 4 \cdot D \cdot t; \langle x\rangle \sim 8$ μm for 1 s at 450 K), global gas phase coupling may, in addition, come into play in the investigated parameter space. Depending on the fraction of the sample surface being in the more reactive oxygen covered state the overall reaction rate varies drastically. A high CO_2 production rate instantaneously diminishes the partial pressures of the educts CO and O_2. Due to the extreme narrowness of the oscillatory or excitable range, small variations in the partial pressures can effectively synchronize the whole surface.[14] In the temperature range below 500 K the difference in reactivity between oxygen and CO-covered state is high so that the intrinsic modulation of the educt partial pressures is strong. Spirals tend to die out after a certain period and to be reborn again, leading to temporal variation of the spiral population across the macroscopic surface area.

The type of spatio-temporal pattern depends on the set of chosen control parameters, p_{O_2}, p_{CO}, and T. In order to rationalize the experimental findings, we restrict ourselves to a two parameter-space spanned by p_{CO} and T, while the O_2 pressure was kept fixed at an arbitrarily chosen value of 4×10^{-4} mbar. The ranges of existence for elliptical reaction-diffusion fronts, of spiral waves and of solitary pulses are depicted in Fig. 2. At low partial pressures of CO the surface is in the oxygen covered state. Increasing the CO pressure leads from the stable state of oxygen covered surface to the threshold of metastability where CO-covered islands start to grow, eventually lose their stability and oxygen fronts nucleate on the growing CO islands. No true bistability is found in the investigated parameter

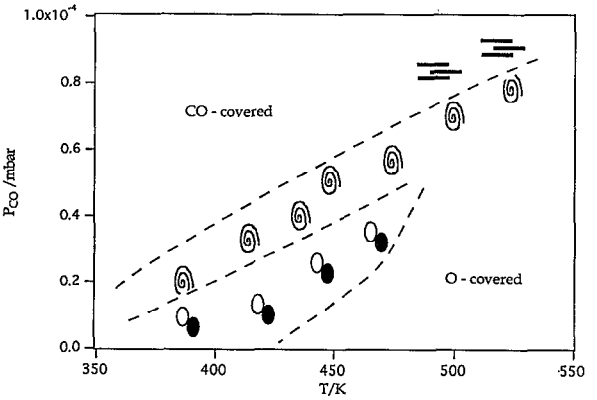

FIG. 2. Experimental bifurcation diagram illustrating the existence ranges for the various spatio-temporal concentration patterns at constant $p_{O_2}=4\times10^{-4}$ mbar as a function of T and p_{CO}. Elliptic reaction-diffusion fronts are characteristic for the metastable regime. Spirals are formed in the range of excitability. At the limit of low excitability (high p_{CO} and high T) the intrinsic core of the spiral diverges and flat solitary waves may be formed as symbolized by parallel bars.

range. At low temperatures the interval of CO partial pressures exhibiting metastable behavior widens. At higher temperatures the existence range narrows and vanishes at $\sim$480 K. Further rise of the CO pressure leads to excitability and the growth of oxygen spiral waves. At even higher CO pressure a narrow range of low excitability is reached, spirals disappear in favor of solitary oxygen pulses.[2] Also meandering of the spiral tip along floral trajectories is theoretically predicted and experimentally found in some other off-equilibrium chemical systems.[15,16] In principle the detachment of the spiral tip from the stable elliptical core might occur in the case of the CO-oxidation but was difficult to observe because of the narrowness of the range of excitability, the tendency of the spiral to pin to surface defects reduces the core size and suppresses meandering. The size of the core is predicted to increase with temperature, so that meandering will be probably more distinct at temperatures above 450 K.

In the limit of high CO pressure the surface is fully CO-saturated because of the inhibition of oxygen adsorption at high CO coverages.

It should be mentioned, that the experimental conditions are favorable for faceting initiated by the periodic structural transformation of the Pt surface which increases the sticking probability for oxygen.[17] The time scale of this process is $\sim$10 min at 450 K. As a consequence steady-state was reached only after a period of time of this order.

Over the full temperature range depicted in Fig. 2 the anisotropy of spiral growth is nearly constant. The spatial ellipticity reflecting the ratio of velocities parallel and perpendicular to the densely packed atomic rows along the [110]-direction of the Pt(110) surface is $\sim$1.8, indicating an anisotropy of the CO diffusion coefficient $D_{110}/D_{001}\approx3$.

B. Propagation of reaction-diffusion fronts

Figure 1 shows a set of PEEM images reflecting the nucleation and growth of elliptically shaped CO waves

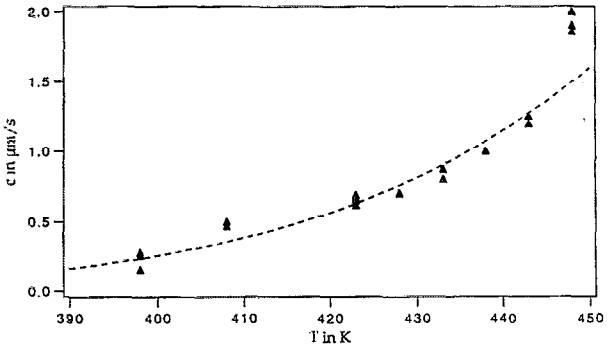

FIG. 3. Variation of the propagation velocity of CO-fronts along the [110]-direction with temperature. The broken line represents a fit with Eq. (1) by using the parameters indicated in the text.

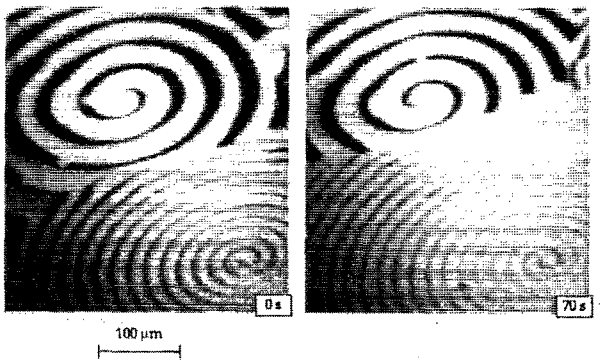

FIG. 4. Coexistence of two spirals with different rotation period and wavelength at 448 K, $p_{O_2}=4\times10^{-4}$ mbar and $p_{CO}=4.3\times10^{-5}$ mbar. The long-wavelength spiral rotates with a period of $T=25.3$ s around an elliptical core of $\sim17\times9$ μm. The short-wavelength spiral rotates with a period of $T=12.8$ s around an elliptical core of $\sim8\times5$ μm.

propagating into an O covered region. For a given temperature the velocity of propagation, c, still varies over a certain range, c_{min} to c_{max}, depending on the additional control parameters, viz., the partial pressures of CO and O_2. From a whole series of experiments, the maximum velocity c_{max} along the [110]-direction at a given temperature T was derived as a function of T. The resulting data are reproduced in Fig. 3.

The propagation velocity of a reaction-diffusion wave is predicted to be given by[18,19]

$$c(T)\approx\sqrt{k(T)}\cdot D(T), \tag{1}$$

where D is the diffusion coefficient of the most mobile species (in the present case CO_{ad}) and $k(T)$ an effective first order rate constant which for our system may be identified with the surface reaction $CO_{ad}+O_{ad}\rightarrow CO_2$. (Desorption of CO is much slower over the temperature range under investigation.) The diffusion coefficient for CO on Pt(110) was recently determined to be associated with an activation energy of 10.1 ± 0.4 kcal/mol and a pre-exponential $D_0=6\times10^{-3}$ cm^2/s.[20] If the activation energy for the surface reaction is assumed to be of the order 10 kcal/mol, Eq. (1) yields a temperature dependence represented by the broken line in Fig. 3 which fits fairly the experimental data between 400 and 440 K, while deviations occur at even higher temperatures.

The propagation velocity of a reaction diffusion front depends on the local curvature, $c=c_0-D\cdot\kappa$, where D is the diffusion coefficient, κ the curvature, and c_0 the velocity of the flat front.[21] At a certain threshold of CO partial pressure waves start to grow on the O_{ad} covered surface with velocities exceeding a threshold value c_{min}. This minimal velocity is different from zero due to the finite size of the nucleation centers available on the surface. Small defects can only trigger fronts with a velocity exceeding the curvature limitation $D\cdot\kappa$; only those fronts for which $c_0-D\cdot\kappa>0$ start to spread. If the diffusion coefficient is known, the onset of front nucleation associated with the minimal observed front velocity c_{min} yields the critical size of the defect from which this front was born. At 448 K CO-fronts within a velocity interval ranging from 1.8 to 2.1 μm/s along the [110]-direction are observed. The minimal observed velocity corresponds to the largest nucleation defect present on the investigated surface area. With the diffusion constant of the CO_{ad}-species, D_{CO} (448 K)$=4\times10^{-8}$ cm^2/s the largest active defect can be correlated to a curvature of $\kappa=0.45$ μm^{-1} corresponding to a defect radius of 2.2 μm.

Strongly curved reaction diffusion fronts show deviations from a constant growth rate and allow, in principle, an estimate to be made of diffusion constants under reaction conditions from the linear relationship between the curvature and the normal propagation velocity.[22] The scatter of the experimental data allows, however, no reasonable analysis for the present system.

C. Spiral waves

A spiral wave may be created if the front of a plane wave breaks up. This may most readily occur in the region of an extended defect exhibiting different kinetic parameters, but free spirals may also be formed from a nonuniform initial distribution in a homogeneous medium. In the latter case without local defects all spirals will exhibit identical rotation periods and spatial wavelengths determined by the external control parameters. At defects the kinetic parameters (e.g., oxygen sticking coefficient) will locally be modified. Such defect regions may act as the cores of spirals and may give rise to a whole distribution of rotation periods and wavelengths.

The two snapshots presented in Figs. 4(a) and 4(b) give an impression of the variety of coexisting spirals with different wavelengths and rotation periods. The faster rotating spiral has a period $\tau=12.8$ s and spatial wavelength of 20.2 μm along the [110]-direction and 12.2 μm along the [001]-direction. The slower spiral rotating with a period of 25.3 s has spatial wavelengths of 40.7 μm, respectively, 26.7 μm along the different directions. Two colliding oxygen pulses annihilate each other and the spiral with shorter rotation period will eventually suppress the one with longer rotation period. The difference of wavelength along the two surface directions again reflects the anisotropy of diffusion. The diffusion coefficient for adsorbed CO is

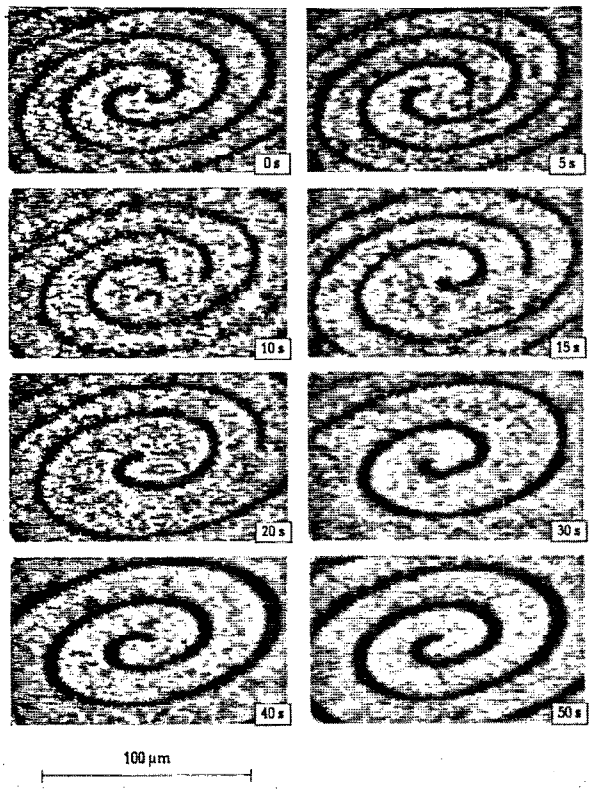

FIG. 5. A double armed spiral relaxes to a simple one armed spiral (T=473 K, $p_{O_2}=4\times10^{-4}$ mbar, $p_{CO}=7.2\times10^{-5}$ mbar).

about three times larger in the [110]-direction (along the missing row structure) than in the perpendicular [001]-direction (see above).

Multiarmed spirals are frequently observed at defects large enough to pin more than one arm. As an example, Fig. 5 shows a two-armed spiral rotating around a distinct defect zone which eventually relaxes to a single-armed spiral. Extended defects were in fact found to act as sources for spirals with even up to 20 arms (Fig. 6)! Multiarmed spirals in a homogeneous medium can in principle be created by transient introduction of a local perturbation which is switched off again after the spiral arms established their regular rotation. Without such external manipulation the formation of multiarmed spirals in homogeneous media is, however, rather improbable and will hence be restricted to defect regions.

The sequence of images in Fig. 7 demonstrates the temporal evolution of four spirals with markedly different properties. The spiral with the longest wavelength and rotation period is completely annihilated by the short wavelength spiral growing out from the left-hand corner. Remarkably the defect forming the core of the extinguished spiral is still discernible as a region of altered reactivity. The wave fronts of the short wavelength spiral break up upon collision with this defect, but are restored again afterwards.

A cut along a line starting at the core of a spiral yields a periodic sequence of concentration pulses separated from

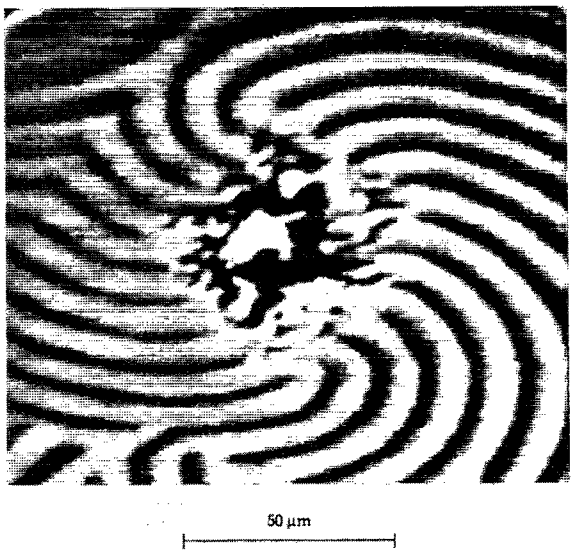

FIG. 6. A 20-armed spiral rotating around a large defect is shown in this picture (T=463 K, $p_{O_2}=4\times10^{-4}$ mbar, $p_{CO}=5.6\times10^{-5}$ mbar).

each other by a wavelength λ and propagating with a velocity c.

The kinetic model developed for the catalytic CO oxidation on Pt(110) was previously solved for a description of the propagation of concentration waves.[23] As can be seen from the theoretical results of Fig. 8, a wave of adsorbed oxygen spreads over a CO-covered surface being essentially present as 1×1-phase. The coverages of O and CO are closely coupled, and as a consequence of the local lowering of CO coverage the surface structure tends to

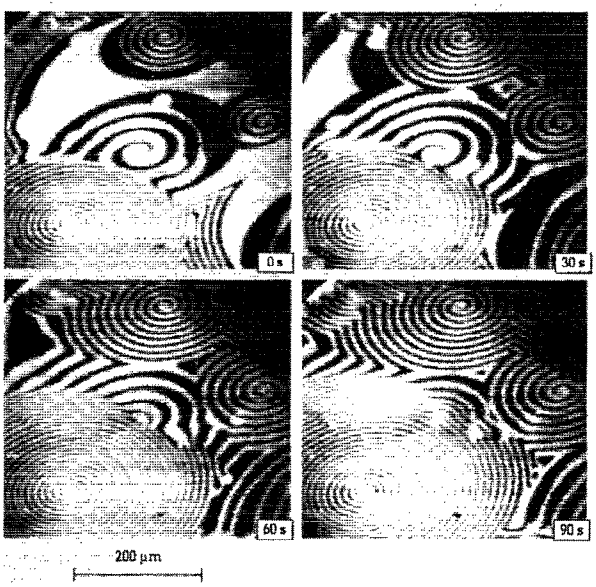

FIG. 7. Temporal evolution of a population of spirals with strongly differing rotation periods and wavelengths at T=448 K, $p_{O_2}=4\times10^{-4}$ mbar and $p_{CO}=4.3\times10^{-5}$ mbar. The core size of the central spiral with large wavelength is 25×14 μm. The spiral annihilating the latter rotates around a core of about 5×3 μm.

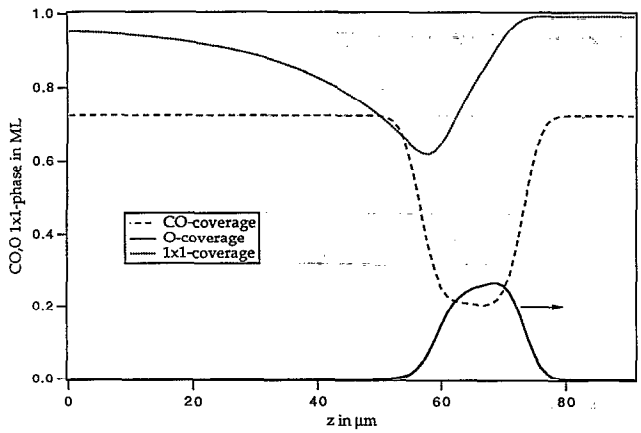

FIG. 8. Calculated data from a one-dimensional reaction diffusion model illustrate the spread of a single oxygen pulse on a CO-covered surface. The coverages of oxygen and carbon monoxide are coupled and the build up of the 1×2 coverage acts as reaction-inhibitor (Ref. 23).

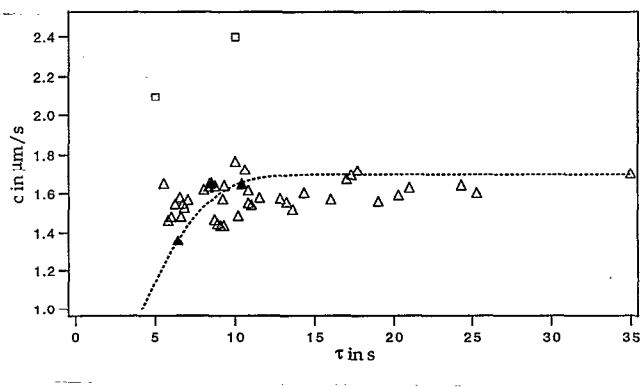

FIG. 9. Distribution of rotation periods and propagation velocities along [110] of spirals observed at fixed control parameters (T=448 K, $p_{O_2}=4\times10^{-4}$ mbar, $p_{CO}=4.3\times10^{-5}$ mbar). The experimental data points are arranged in a $c(\tau)$-dispersion relation.

transform back into the 1×2-phase with a delay determined by the kinetics of this phase transformation. This effect causes a local lowering of the sticking coefficient for oxygen adsorption and hence the O coverage drops thus producing a single wave pulse. This figure illustrates further the origin of a refractory region behind the wave pulse over which the excitable CO-covered 1×1-phase is restored.

If the temporal sequence of pulses in a periodic wave train is long enough ($\tau \gg$ recovery time), consecutive pulses will not interact with each other and their propagation velocity will be independent of their wavelength λ. Otherwise the wave front of each pulse will experience a region of lower excitability caused by the preceding pulse leading to a reduction in propagation velocity c. As a consequence there will exist a dispersion relation $c(\lambda)$, respectively $c(\tau)$, where the period $\tau=\lambda/c$. The period or wavelength of a spiral will be influenced by the nature of the defect zone forming the core of the spiral, as becomes evident, e.g., from inspection of Fig. 8.

A large number of spirals recorded at a fixed set of control parameters (T=448 K, $p_{CO} = 4.3 \times 10^{-5}$ mbar, $p_{O_2} = 4 \times 10^{-4}$ mbar) was analyzed in terms of their rotation periods and wavelength leading to the dispersion relations $c(\tau)$ reproduced in Fig. 9. The data for spirals with long rotation periods and long wavelength correspond to high propagation velocity; for the indicated control parameters $c_{max} = 1.6\ \mu$m/s along the [110]-direction and 0.9 μm/s along the [001]-direction were derived, respectively.

All spiral waves with periods > 15 s were found to be attached to a surface defect discernible in the PEEM image, while those with shorter periods are pinned to cores which can no longer be imaged or are even free spirals on homogeneous regions of the surface. The pronounced spread in wavelength (period) of the spirals has clearly to be attributed to the differing properties of the defect zones forming their cores.

The scatter of the data points in Fig. 9 is mainly caused by a slight drift of the control parameters during the extended period of several hours during which the images were recorded which markedly influence the dynamics. Nevertheless there is a clear trend as indicated by the broken line. Spirals with short wavelengths (=periods τ) are associated with lower velocities of propagation, while for $\tau > 10$ s the velocity is practically constant, i.e., the system is then essentially without dispersion. This statement is corroborated by data taken from different spirals on the same images for which the control parameters were definitely identical and which are marked in Fig. 10 by full triangles. Strikingly the two data points dating from an earlier measurement (open rectangles) at identical choice of the control parameter do not fit well into the dispersion curve. This effect can be related to the history of the single crystal, which was polished between the two measurements. A miscut of 0.5° (error for standard single crystal preparation) leads to more than 20 monoatomic steps per μm. Diffusion is very sensitive to the morphology of the surface. Faster diffusion increases the front velocity. Significant dispersion however is observed in the same interval of rotation periods.

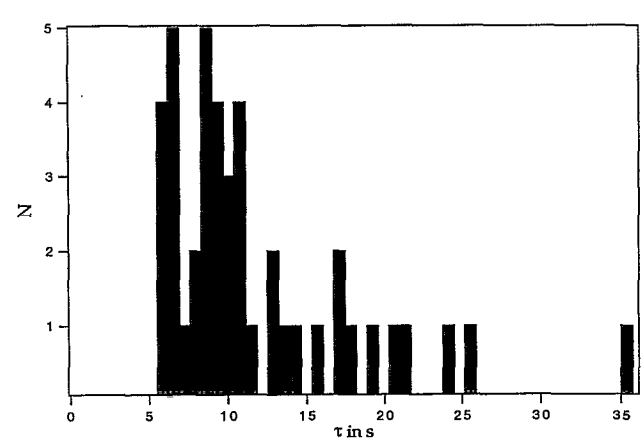

FIG. 10. Histogram for the spirals found at T=448 K, $p_{O_2}=4\times10^{-4}$ mbar and $p_{CO}=4.3\times10^{-5}$ mbar during a scan over the macroscopic surface of the single crystal sample.

The qualitative features of the dispersion relation for the present system are in agreement with the arguments presented above and closely resemble results reported previously for the Belousov–Zhabotinskii (BZ) reaction[24] and as also reproduced in a theoretical study by Keener and Tyson[25] based on the Oregonator model for this reaction.

Analysis of a large number of spirals yields the histogram of Fig. 10 representing the abundances of spirals within a certain range of periodicity. It turns out that spirals with small periods (=wavelengths) are more frequent than those with longer τ. The latter events are associated with more extended defect zones forming the cores, while "free" spirals not pinned to a defect are associated with short periods. It should be noted that spirals of the latter type are presumably somewhat over represented in the histogram of Fig. 10, since large wavelength spirals are annihilated to some extent by interfering short wavelength spirals as outlined above. The maximum in Fig. 10 occurs roughly for $\tau \approx 8$ s. This corresponds to a wavelength of ~ 13 μm and the core radius is estimated to be of the order 1 μm. Events in this range are tentatively identified with "free" spirals. It should be mentioned that the free spiral is not necessarily associated with the shortest period. Diffusion flux may be reduced in the region of a defect, and the conditions for front propagation are similar to those for a straight, unbroken front. At the boundary of the defect the front curvature may hence exceed the critical value needed at the end of a free spiral. It was shown that for these reasons under certain conditions the core size of a free spiral may be larger by up to $\sim 20\%$ than that of the defect causing the spiral with shortest period.[26]

Influences of the curvature on front propagation velocity come generally only into play if $D \cdot \kappa$ (κ=curvature) is of the same order of magnitude as the velocity c_0 of the flat front. With the data for the present system it is estimated that such an effect will have to be taken into account for front radii below ~ 10 μm which are only found in the immediate vicinity of the cores or at the sharp ends of the cusplike structures formed after collision of two spirals. Detailed analysis of the temporal evolution of such features offers in principle a possibility to derive information about diffusion coefficients under reaction conditions.[22]

Drifting of a spiral may be initiated by controlled variation of excitability either in time or space.[27] For the BZ reaction convenient ways were found by using a photosensitive ruthenium compound catalyst[28] or by applying an electric field to the reacting solution.[29] Experiments of this type were performed by periodically modulating the intensity of light illuminating the photosensitive solution reacting in a Petri dish,[30] and by applying a gradient of light intensity.[31]

Periodic variation of the excitability of the medium by external modulation of one of the control parameters affects the affinity of a free spiral tip to wind up. As a consequence the tip starts to travel along a trajectory determined by the rotation of the undisturbed spiral (with frequency ω_0) and by the frequency ω (and phase) of the perturbation. The 1:1 resonance case ($\omega=\omega_0$) was treated theoretically by Mikhailov[27] for small amplitudes of perturbation within the framework of the kinematical approximation.

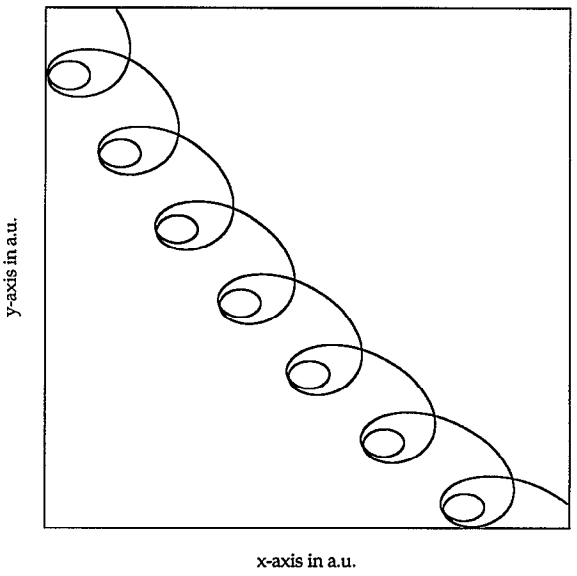

FIG. 11. Calculated trajectories of the tip motion under the effect of external periodic perturbation. The path is calculated close to the 1/2 resonance. The curve has been generated through direct integration of the reduced kinematical equations. The critical curvature controlling the spread of the spiral tip has been modulated with an amplitude of 60%.

Calculations using the same approximation were performed for the near 1:2 resonance case ($\omega_0=0.505\ \omega_0$) in order to model the experiments to be described below. The resulting trajectory of the spiral tip is reproduced in Fig. 11. The gross motion follows almost a straight line to which small double loops are superimposed as fine structure. (For the 1:1 case these would be single loops.)

Experiments on spiral drift with the present system where performed by modulating the temperature, $T=T_0 + 1/2\Delta T \sin(\omega t)$. Since the effects under discussion are restricted to the motion of free spirals, the control parameters had to be selected in a way that the core size of free spirals exceeded the average diameter of surface defects so that core pinning became improbable. This is achieved for conditions of relatively low excitability where the oxygen wave pulses are rather narrow. The data to be presented were recorded at constant $p_{CO} = 1.2 \times 10^{-5}$ mbar, $p_{O_2}=4\times 10^{-4}$ mbar, with $T_0=398$ K and $\Delta T=1$ K at $\omega=0.05\ s^{-1}$. The (average) rotation frequency of the free spiral was determined to be $\omega_0=0.1\ s^{-1}$, so that the conditions were close to the $\omega/\omega_0=1/2$ resonance.

A series of PEEM images of a spiral recorded at different stages of the modulation is reproduced in Fig. 12. Because of the 1:2 resonance conditions, the modulation of excitability has a pronounced effect on the shape of the spiral near its tip. The average drift velocity of the core (~ 0.35 μm/s) is of the same order of magnitude as the average velocity of rotation of the tip around its core (~ 0.15 μm/s). As a consequence the shape of the spiral is strongly distorted and exhibits a pronounced Doppler effect in that the wavelength is compressed along the drift direction and expanded in the reverse direction. This is

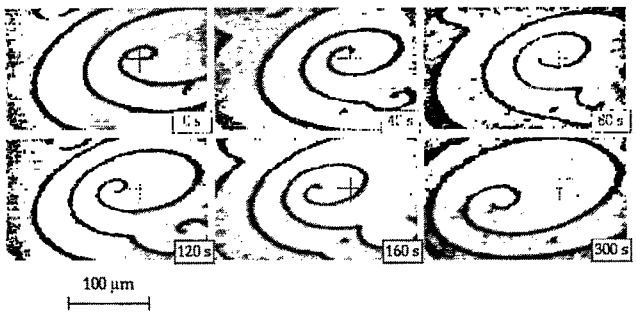

FIG. 12. Spiral wave drifting under the influence of modulated temperature (T_0=398 K, ΔT=1 K, ω=0.05 s^{-1}, $p_{O_2}=4\times10^{-4}$ mbar, $p_{CO}=1.8\times10^{-5}$ mbar).

because the drift velocity is about one third of the wave propagation velocity in [110]-direction ($\sim$0.9 μm/s).

Figure 13(a) shows the coarse trajectory of the tip motion recorded in intervals of 20 s. For ω/ω_0 being exactly 1/2 (or generally, $1/n$) the tip would move along a straight line. Otherwise the trajectory is predicted to follow a circle whose radius is proportional to the difference $|n\cdot\omega-\omega_0|$ (Ref. 27) which is obviously the case for the present conditions. In addition one expects a fine structure of the motion of the tip in that it performs single (n=1) or double (n=2) loops along the gross path, as outlined above.

A plot of the positions of the tip recorded in intervals of 4 s is reproduced in Fig. 13(b). The conditions of temporal and spatial resolution are not yet sufficient to completely resolve this loop structure; the exact location of the tip is limited to an area of $\sim10\times10$ μm^2. However the more or less irregular features in this trajectory are not due to random motions but clearly indicated the presence of a fine structure of the discussed type.

IV. CONCLUSIONS

Several types of spatio-temporal concentration patterns are associated with the catalytic CO oxidation on a Pt(110) surface for conditions outside the oscillatory regime and existence regions for the different patterns were determined for a fixed O_2 partial pressure (4×10^{-4} mbar) as a function of CO partial pressure and of temperature; growing elliptic wave fronts, spirals, and solitary wave pulses. The latter phenomena were discussed in detail elsewhere.[2,32] Additional qualitatively different phenomena might be expected upon more detailed analysis of the parameter space. For example, at temperatures >450 K expanding spiral cores and strongly "meandering" spirals might be formed which eventually give rise to the phenomenon of "spiral turbulence."

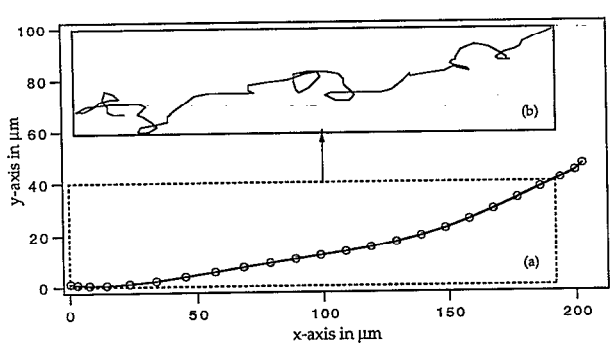

FIG. 13. Trajectory of the tip. The coarse path (a) is recorded with Δt=20 s. At higher temporal resolution a fine structure becomes apparent (b).

The evolution of elliptic wave fronts is closely related to the nucleation and growth of propagating patterns in a bistable medium as, e.g., characteristic for the same reaction occurring on a Pt(111) surface,[5,33] with the important difference that with the present system no real bistability exists and hence the two states (predominantly O or CO-covered) are only metastable. If, for example, one starts with a situation in which the surface is uniformly mainly covered by oxygen and increases the CO partial pressure after passing a certain threshold, elliptically shaped CO islands nucleate and grow. {The elliptical shape is a consequence of the anisotropy of the diffusion coefficient of adsorbed CO which in the temperature range under discussion differs by about a factor of 3 between the [110]- and [001]-directions of the Pt(110) surface.} After some time the CO patches lose stability and O domains nucleate and grow. The velocity of front propagation has a nonvanishing threshold value which indicates the participation of surface defects. Only fronts can grow whose velocities exceed the threshold $D\cdot\kappa$, where D is the diffusion coefficient and κ the local curvature. The linear relation between front propagation velocity and κ offers, in principle, a straightforward possibility to determine D under reaction conditions. The temperature dependence of the front propagation velocity yields an activation energy of $\sim$10 kcal/mol which is compatible with estimates based on the relation $c\propto\sqrt{k\cdot D}$ (k=effective first order rate constant) holding for simple reaction-diffusion systems.

Spiral waves were generally found at higher CO partial pressures than the elliptical front waves. Their properties were investigated in some detail for a fixed set of control parameters (T=448 K, $p_{CO}=4.3\times10^{-5}$ mbar, $p_{O_2}=4\times10^{-4}$ mbar). Even for constant control parameters a variety of spirals (including multiarmed spirals) may be observed. This has to be attributed to the fact that apart from "free" spirals in a homogeneous medium, cores may be readily pinned to defect zones on the surface whose properties (in particular lateral extensions) determine the spiral dynamics.

The front propagation velocity c of spiral waves varies with their period τ (which is related with the wavelength λ through $\tau=\lambda/c$) in a way that c at first increases with τ, but soon reaches a constant value of $c_{max}\approx1.6$ μm/s as rationalized on the basis of qualitative arguments. The period of the free spiral (whose core is not pinned to a defect) is $\sim$8 s, and its wavelength $\sim$12 μm under the quoted conditions. Effects of the curvature of the concentration spirals on the propagation velocity will be restricted to regions very close to the core or to the sharp cusp-type structures originating from the collision of spiral waves.

If the conditions are chosen in a way that the core size of the "free" spiral exceeds the average defect size, spirals can be forced to drift across the surface by periodic modulation of one of the control parameters. This was exemplified by modulating the temperature ($T_0=398$ K) with an amplitude of 1 K and with a frequency near 1/2 of the rotation frequency of the spiral. The conditions near resonance caused a fairly high drift velocity (~ 0.35 μm/s) comparable to the propagation velocity of the spiral fronts along the [110]-direction (~ 0.9 μm/s) as manifested by a pronounced Doppler-effect for the spiral wavelengths.

ACKNOWLEDGMENTS

Fruitful and stimulating discussions with M. Bär and A. S. Mikhailov are gratefully acknowledged.

[1] S. Jakubith, H. H. Rotermund, W. Engel, A. von Oertzen, and G. Ertl, Phys. Rev. Lett. **65**, 3013 (1990).
[2] H. H. Rotermund, S. Jakubith, A. von Oertzen, and G. Ertl, Phys. Rev. Lett. **66**, 3083 (1991).
[3] G. Ertl, Science **254**, 1750 (1991).
[4] T. Engel and G. Ertl, Adv. Catal. **28**, 1 (1979).
[5] M. Bär, C. Zülicke, M. Eiswirth, and G. Ertl, J. Chem. Phys. **96**, 8595 (1992).
[6] M. Eiswirth and G. Ertl, Surf. Sci. **122**, 90 (1986).
[7] K. Krischer, M. Eiswirth, and G. Ertl, J. Chem. Phys. **96**, 9161 (1992).
[8] W. Engel, M. E. Kordesch, H. H. Rotermund, S. Kubala, and A. von Oertzen, Ultramicrosc. **36**, 148 (1991).
[9] A. von Oertzen, H. H. Rotermund, S. Jakubith, and G. Ertl, Ultramicrosc. **36**, 107 (1991).
[10] H. H. Rotermund, S. Nettesheim, A. von Oertzen, and G. Ertl, Surf. Sci. **275**, L645 (1992).
[11] C. Zülicke, A. S. Mikhailov, and L. Schimanski-Geier, Physica A **163**, 559 (1990).
[12] R. Gomer, Rep. Prog. Phys. **53**, 917 (1990).
[13] M. Bär, thesis FU Berlin, 1993 (in preparation).
[14] M. Eiswirth, P. Möller, K. Wetzl, R. Imbihl, and G. Ertl, J. Chem. Phys. **90**, 510 (1989).
[15] W. Jahnke and A. T. Winfree, Int. J. Bifurc. Chaos **1**, 445 (1991).
[16] T. Plesser, S. C. Müller, and B. Hess, J. Phys. Chem. **94**, 7501 (1990).
[17] S. Ladas, R. Imbihl, and G. Ertl, Surf. Sci. **197**, 153 (1988).
[18] R. Luther, Z. Elektrochem. **12**, 596 (1906).
[19] K. Showalter and J. J. Tyson, J. Chem. Educ. **64**, 742 (1987).
[20] A. von Oertzen, thesis FU Berlin, 1993 (in preparation).
[21] A. Nitzan, P. Ortoleva, and J. Ross, Faraday Symp. Chem. Soc. **9**, 241 (1974).
[22] P. Foerster, S. C. Müller, and B. Hess, Science **241** 685 (1988).
[23] M. Falcke, M. Bär, H. Engel, and M. Eiswirth, J. Chem. Phys. **97**, 4555 (1992).
[24] A. Pagola, J. Ross, and C. Vidal, J. Phys. Chem. **92**, 163 (1988).
[25] J. J. Tyson and J. P. Keener, Physica D **32**, 327 (1988).
[26] A. S. Mikhailov and V. S. Zykov, Physica D **52**, 379 (1991).
[27] A. S. Mikhailov, *Foundations of Synergetics I* (Springer, Berlin, 1990).
[28] L. Kuhnert, Nature **319**, 393 (1986).
[29] O. Steinbock, J. Schütze, and S. C. Müller, Phys. Rev. Lett. **68**, 248 (1992).
[30] K. I. Agladze, V. A. Davydov, and A. S. Mikhailov, Sov. Phys. JETP Lett. **45**, 601 (1987).
[31] M. Markus, Z. Nagy-Ungvarai, and B. Hess, Science **257**, 225 (1992).
[32] M. Bär, M. Eiswirth, H. H. Rotermund, and G. Ertl, Phys. Rev. Lett. **69**, 945 (1992).
[33] M. Ehsasi (personal communication).